ADVANCES IN ATMOSPHERIC SCIENCES, VOL. 36, MARCH 2019, 279–291

• **Original Paper** •

Global Monsoon Changes under the Paris Agreement Temperature Goals in CESM1(CAM5)

Xia QU*[1,2,3] and Gang HUANG[1,3]

[1] *Center for Monsoon System Research, Institute of Atmospheric Physics, Chinese Academy of Sciences, Beijing* 100029*, China*

[2] *State Key Laboratory of Numerical Modeling for Atmospheric Sciences and Geophysical Fluid Dynamics, Institute of Atmospheric Physics, Chinese Academy of Sciences, Beijing* 100029*, China*

[3] *Joint Center for Global Change Studies (JCGCS), Beijing* 100875*, China*

(Received 27 June 2018; revised 11 October 2018; accepted 6 November 2018)

ABSTRACT

Based on experiments with the Community Earth System Model, version 1 (Community Atmosphere Model, version 5) [CESM1(CAM5)], and an observational dataset, we found that CESM1-CAM5 is able to reproduce global monsoon (GM) features, including the patterns of monsoon precipitation and monsoon domains, the magnitude of GM precipitation (GMP, the local summer precipitation), GM area (GMA), and GM percentage (the ratio of the local summer precipitation to annual precipitation). Under the Paris Agreement temperature goals, the GM in CESM1-CAM5 displays the following changes: (1) The GMA is ambiguous under the 1.5°C temperature goal and increases under the 2.0°C temperature goal. The increase mainly results from a change in the monsoon percentage. (2) The GM, land monsoon and ocean monsoon precipitation all significantly increase under both the 1.5°C and 2.0°C goals. The increases are mainly due to the enhancement of humidity and evaporation. (3) The percentages of GM, land monsoon and ocean monsoon feature little change under the temperature goals. (4) The lengths of the GM, land monsoon and ocean monsoon are significantly prolonged under the temperature goals. The increase in precipitation during the monsoon withdrawal month mainly accounts for the prolonged monsoons. Regarding the differences between the 1.5°C and 2.0°C temperature goals, it is certain that the GMP displays significant discrepancies. In addition, a large-scale enhancement of ascending motion occurs over the southeastern Tibetan Plateau and South China under a warming climate, whereas other monsoon areas experience an overall decline in ascending motion. This leads to an extraordinary wetting over Asian monsoon areas.

Key words: global monsoon, Paris Agreement, temperature goals, precipitation

Citation: Qu, X., and G. Huang, 2019: Global monsoon changes under the Paris Agreement temperature goals in CESM1(CAM5). *Adv. Atmos. Sci.*, **36**(3), 279–291, https://doi.org/10.1007/s00376-018-8138-y.

1. Introduction

The 2015 Paris Agreement proposed "Holding the increase in the global average temperature to well below 2°C above pre-industrial levels and pursuing efforts to limit the temperature increase to 1.5°C above pre-industrial levels" (UNFCCC, 2015). To achieve the 1.5°C warming target, the concentrations of greenhouse gases (GHGs) must decline before 2060; whereas the GHG concentrations must decrease before 2085 to realize the 2°C warming target (Sanderson et al., 2016). As the concentrations of GHGs decrease, the global mean temperature (GMT) exhibits warming inertia (Held et al., 2010; Chadwick et al., 2013), which is mainly due to the large capacity of heat storage of the deep ocean (Held et al., 2010). The role of the deep ocean after the decrease in GHG concentrations is quite different to its role when the concentration increases. It leads to a very different ocean surface warming pattern and, consequently, a different climate response in the atmosphere (Chadwick et al., 2013; Long et al., 2014). Thus, climate change under a 1.5°C warming scenario may not be linearly speculated from the results under the +8.5 W m^{-2} Representative Concentration Pathway scenario (RCP8.5), under which the GHG concentrations do not decline.

It must be noted that the Paris Agreement did not specify the trajectory of carbon emissions for realizing the 1.5°C warming goal and that a slight exceedance of 1.5°C before 2100 is permitted. A previous study demonstrated that different trajectories of GHG radiation that reach a 2°C warming result in different regional responses in precipitation (Good et al., 2016). Therefore, climate change in a 1.5°C warming world is likely subject to the trajectories of GHG radiation.

Monsoon climates display strong seasonality, convention-

* Corresponding author: Xia QU
Email: quxia@mail.iap.ac.cn

ally characterized by a distinct wet summer and dry winter. Across the globe, areas affected by monsoons account for approximately 20% of Earth's surface, and the monsoon precipitation accounts for 30.8% of all precipitation (Wang and Ding, 2008). Moreover, more than two-thirds of the world's population lives in monsoon areas. The variability of monsoon precipitation may exert profound social and economic influences on people that live in monsoon areas.

The global monsoon (GM) displays some responses to a warming world. Under the RCP4.5 scenario, CMIP5 results show that the GM area will not change significantly; the GM onset will be advanced, and its withdrawl will be delayed (Lee and Wang, 2014); and the GM precipitation will increase, primarily led by increases in moisture convergence and surface evaporation (Hsu et al., 2013).

However, the GMT increase suggested by CMIP5 models under RCP4.5 at the end of the 21st century will be above 2.0°C (Good et al., 2016), and is different from the temperature goal of the Paris Agreement. Even the GMT in the multi-model mean of the RCP2.6 experiment, the lowest emission scenario, is above 1.5°C in 2100 (Wang et al., 2017). Thus, the GM behaviors under the 1.5°C temperature goal are not clear. Recently, the Community Earth System Model, version 1 (Community Atmosphere Model, version 5) [CESM1(CAM5)] conducted a "low warming" experiment (Sanderson et al., 2017), which may be the first set of simulations whose GMT increase is 1.5°C at 2100 relative to the pre-industrial level. To compare to climate change when the GMT increase is 2.0°C, "2.0°C warming" experiments are also conducted. By analyzing the outputs of CESM1(CAM5), this study intends to address the following problems: Will GM characteristics change significantly below the 1.5°C temperature goal? Will the characteristics display significant discrepancies below 1.5°C compared to the 2.0°C temperature goal?

Section 2 introduces the data and methods of the present study. Section 3 assesses the reproducibility of CESM1(CAM5) in terms of GM features. Section 4 discusses the future change in GM, as well as ocean and land monsoons, under the Paris Agreement temperature goals. Section 5 is a summary and discussion.

2. Data and methods

The study presented herein is mainly based on experiments of CESM1(CAM5). CESM1(CAM5) is composed of coupled atmosphere, ocean, land, and sea-ice component models. The horizontal resolutions of all the model components is approximately 1°. It includes the atmospheric carbon dioxide cycle, the land carbon cycle and ocean biogeochemistry. It is introduced in more detail in Kay et al. (2015) and Sanderson et al. (2017). The experiments used for this study are:

(1) Large ensemble experiment (LE). Ensemble 1 of the LE experiment is forced by well-mixed GHGs, short-lived gases and aerosols and ozone from 1850–2005. Ensemble 2 is driven by the same forcing as ensemble 1, but from 1920–2005; its initialization is the same as that used for 1 January 1920 of ensemble 1, but the ocean temperatures are lagged by one day. Ensembles 3–35 are driven by the same forcing as ensemble 2; their initializations are the same as that used for 1 January 1920 of ensemble 1, except for the air temperature with round-off (order of 10–14 K) differences.

(2) 1.5°C warming (never exceeding) experiment (1.5NE). In this scenario, the expected multi-year GMT never exceeds 1.5°C above pre-industrial levels (1850–1920 mean). Before 2017, emissions are the same as RCP8.5. After 2017, carbon emissions rapidly decline and reach half of the 2017 levels in 2027. The net combined carbon emissions decrease to zero in 2038. Carbon emissions reach a peak net negative level (-1.8 GtC yr^{-1}) in 2065. After this, negative emission fluxes are reduced, reaching -0.9 GtC yr^{-1} by 2100.

(3) 1.5°C warming (overshoot) experiment (1.5OS). In this experiment, the expected GMT is slightly overshot before returning to 1.5°C by 2100. The emissions are the same as in 1.5NE, with the exception of the following cases: (a) after 2017, emissions decrease slightly less rapidly than those in 1.5NE and reach halves of 2017 levels in 2032; (b) net combined carbon emissions reach zero in 2046; (c) after 2046, the corresponding fluxes of negative emissions are greater than than those in 1.5NE and reach a peak (-4.0 GtC yr^{-1}) in 2080; and (d) after 2080, negative emissions are rapidly reduced and reach -1.0 GtC yr^{-1} in 2100.

(4) 2.0°C warming (never exceeding) experiment (2.0NE). The experiment is the same as 1.5NE except for the following: (a) the expected multi-year GMT never exceeds 2.0°C; (b) after 2017, the emissions decrease much less rapidly than in 1.5NE and reach halves in 2042; (c) net combined emissions reach zero in 2078; (d) then, negative emissions occur and reach a peak net negative flux (-0.8 GtC yr^{-1}) in 2120.

The LE, 1.5NE, 1.5OS and 2.0NE experiments respectively include 35, 10, 5 and 10 members. The information for the LE experiment is introduced in Kay et al. (2015) in detail, whereas the 1.5NE, 1.5OS and 2.0NE experiments are introduced in Sanderson et al. (2017). The global mean surface temperature during 2071–2100 is 1.07°C, 1.16°C and 1.58°C in the 1.5NE, 1.5OS and 2.0NE experiments, respectively, relative to that during 1980–2005 in the LE experiment. The total precipitation is the sum of convective precipitation and large-scale precipitation. Evaporation is absent in CESM1(CAM5) outputs and is computed from the surface latent heat flux.

The observational data that are used to evaluate the reproducibility of CESM1(CAM5) include the (1) Global Precipitation Climatology Project (GPCP), version 2.3 (Adler et al., 2003), and (2) Center for Climate Prediction Merged Analysis of Precipitation (CMAP; Xie and Arkin, 1997). Both sets of precipitation data have a 2.5° horizontal resolution. Here, the evaluation focuses on the period from 1980–2005. Since the resolutions of CESM1(CAM5) and observations are inconsistent, we interpolate the observational data into grids that are the same as CESM1(CAM5).

The model reproducibility is assessed based on the S-index (Taylor, 2001; Hirota et al., 2011), defined as

$$S = \frac{(1+R)^4}{4\left(\mathrm{SDR} + \frac{1}{\mathrm{SDR}}\right)^2}, \quad (1)$$

where R is the spatial correlation and SDR is the spatial standard deviation in CESM1(CAM5) against that in the observation. Supposing that the evaluated variable is the same in CESM1(CAM5) and in the observation (R equals 1.0 and SDR equals 1.0), we can speculate that the best reproducibility corresponds to $S = 1.0$.

In addition, we employed the Student's t-test to evaluate the significance level of different samples. The standard deviation used in the test is the inter-ensemble spread.

3. Climatology of the GM in CESM1(CAM5)

Monsoon climates feature wet summers and dry winters. Precipitation variation is an important factor for measuring it. Following Hsu et al. (2011, 2013) and Lee and Wang (2014), the GM area (GMA) is defined as the domains where the difference between local summer and local winter mean precipitation exceeds 2 mm d^{-1}, and the local summer precipitation accounts for no less than 55% of annual rainfall. In the Northern Hemisphere, the definition of local summer is May to September, and the local winter is November to March; in the Southern Hemisphere, the definition is the reverse. At the equator the precipitation is set to 0. The GM precipitation (GMP) is the local summer mean precipitation; the GM annual range (GMR) is the difference between local summer mean precipitation and local winter mean precipitation; the GM intensity (GMI) is GMR normalized by annual mean rainfall. The GM percentage is defined as the ratio of the local summer precipitation to annual precipitation. In the following, the GMP, GMR, GMI and GM percentage are the area averages of the corresponding variables over the GMA with latitudinal weighting. In this study, we focus on the latitudes between 60°S and 60°N.

Figure 1 displays the climatological distribution of monsoon precipitation and area during 1980–2005. The CESM1(CAM5) LE experiment reproduces the gross features of the GMP well, such as the intertropical convergence zone, the South Pacific convergence zone, the mei-yu/baiu rainbelt and the Indo-Pacific warm pool (Fig. 1). Between 60°S and 60°N, the pattern correlation coefficients (PCCs) between the CESM1(CAM5) LE single experiment and the GPCP range from 0.828 to 0.839, whereas the correlation coefficients between CESM1(CAM5) and CMAP range from 0.832 to 0.844 (Table 1). The S-indices, which measure model reproducibility, between the CESM1(CAM5) LE single experiment and the GPCP range from 0.693 to 0.709, and the indices between CESM1(CAM5) and CMAP range from 0.703 to 0.723. In addition, the GMR, GMI and GM percentage are calculated. The PCCs and S-indices display similar results (Table 1). Thus, CESM1(CAM5) reproduces the global patterns of the features associated with the GM well, whereas the ability to describe the GM's spatial variation is slightly worse than that of the global patterns.

CESM1(CAM5) reproduces most of the monsoon domains well (the GMA is outlined by red lines in Fig. 1), including the Australian monsoon, tropical North African monsoon, South African monsoon, North American monsoon and South American monsoon domains. Over land, the Asian monsoon domain is reasonably reproduced; whereas over ocean, the adjacent western North Pacific monsoon regions are not reasonably simulated. This deficiency is also observed in CMIP5 models (Hsu et al., 2013; Lee and Wang, 2014). In CESM1(CAM5), over the western North Pacific, the ratio of local summer precipitation to annual rainfall is generally less than 0.55 (figure not shown), which leads to the simulation deficiency.

The GMA in GPCP and CMAP is 8.16×10^7 km^2 and 8.48×10^7 km^2, respectively. For the 35 members of the CESM1(CAM5) LE experiment, the GMA ranges from 8.06×10^7 km^2 to 8.51×10^7 km^2. Some members are able to capture the observational GMA, indicating the good reproducibility of CESM1(CAM5) with respect to the GMA.

CESM1(CAM5) reasonably reproduces the mean GMP and GM percentage. The averaged GMP over the GMA in CESM1(CAM5) ranges from 6.14 to 6.29 mm d^{-1}, whereas they are 6.12 mm d^{-1} and 6.28 mm d^{-1} in GPCP and CMAP, respectively (Table 2). The averaged GM percentage over the GMA in CESM1(CAM5) ranges from 70.9% to 71.9%, slightly higher than observed values (70.4% and 70.1% in GPCP and CMAP, respectively). This very small bias is acceptable.

In CESM1(CAM5), the summer–winter rainfall contrast is more prominent. It overestimates the GMR, ranging from 4.76 mm d^{-1} to 4.88 mm d^{-1}, or 3%–6% higher than observations (Table 2). In turn, the overestimated GMR leads to a GMI that is higher than observed [1.36–1.40 in CESM1(CAM5), 1.31 in GPCP and 1.30 in CMAP].

Generally, CESM1(CAM5) reproduces the global pattern of the features associated with the GM well, as well as the GMA and the global mean GMP and GM percentage. Therefore, using CESM1(CAM5) to discuss the future change in GMA, GMP and GM percentage is viable.

Table 1. Ranges of PCCs and S-indices for CEMS1(CAM5) LE experiments and observations.

	GMP		GMR		GMI		GM percentage	
	PCC	S-index	PCC	S-index	PCC	S-index	PCC	S-index
GPCP	0.828–0.839	0.693–0.709	0.817–0.833	0.668–0.693	0.806–0.827	0.664–0.696	0.806–0.827	0.665–0.696
CMAP	0.832–0.844	0.703–0.723	0.787–0.808	0.628–0.657	0.826–0.845	0.695–0.725	0.824–0.843	0.691–0.720

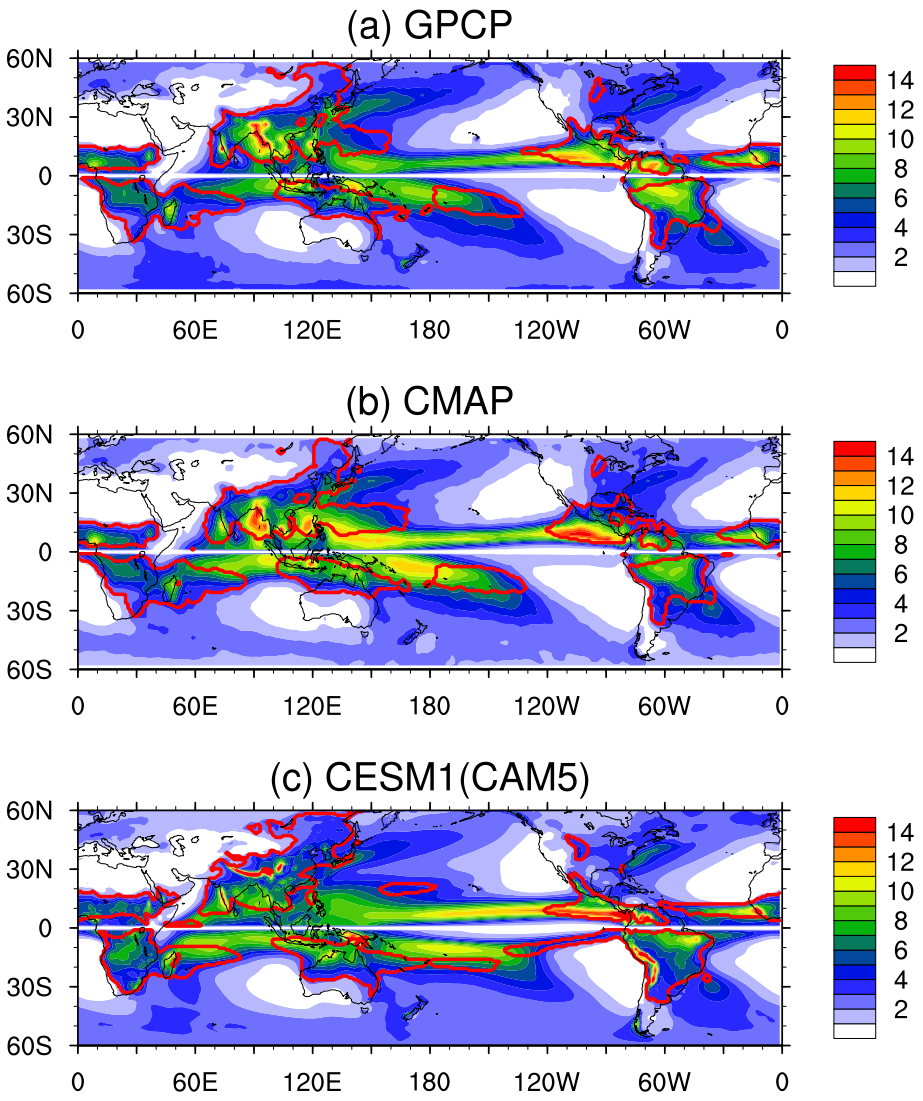

Fig. 1. Climatology of monsoon rainfall (color shading; units: mm d^{-1}) and monsoon area (red lines) in (a) GPCP, (b) CMAP and (c) the multi-EM of the CESM1(CAM5) LE experiment. The monsoon rainfall is the local summer mean rainfall, where local summer is May to September in the Northern Hemisphere and November to March in the Southern Hemisphere. The period is 1980–2005.

Table 2. Area-average GM associated indices over the GMA.

	GMP (mm d^{-1})	GMR (mm d^{-1})	GMI	GM percentage
GPCP	6.12	4.59	1.31	0.704
CMAP	6.28	4.64	1.30	0.701
CESM1(CAM5)	6.14–6.29	4.76-4.88	1.36–1.40	0.709–0.719

4. Future changes in the GM

4.1. *GMA*

To predict future changes, we define the "present day" (LE experiment) as 1980–2005, and the "end of the 21st century" as 2071–2100 (also called "future" for short). To compute GMA differences, two methods are employed: (1) We first compute the ensemble mean (EM) of the climatological precipitation in each scenario; then, the GMAs, as well as their differences, are computed based on the EMs (displayed as bars in Fig. 2). (2) We gain a GMA from the climatological precipitation in each ensemble, and then the mean GMA is computed in each scenario. Finally, the differences are obtained by comparing mean GMAs between scenarios (displayed in Fig. 2 as solid circles and error bars). The GMA differences based on the two methods are slightly different, but the gross changes are similar. Compared to present-day climate, the gross GMAs significantly expand under 1.5OS and 2.0NE (approximately 1.7%), whereas little change occurs under 1.5NE (Figs. 2a–c). Interestingly, despite nearly the same GMT change in 2100, different carbon emissions lead to different GMA changes. If the GMT increase relative to the pre-industrial level reaches both 1.5°C and 2.0°C

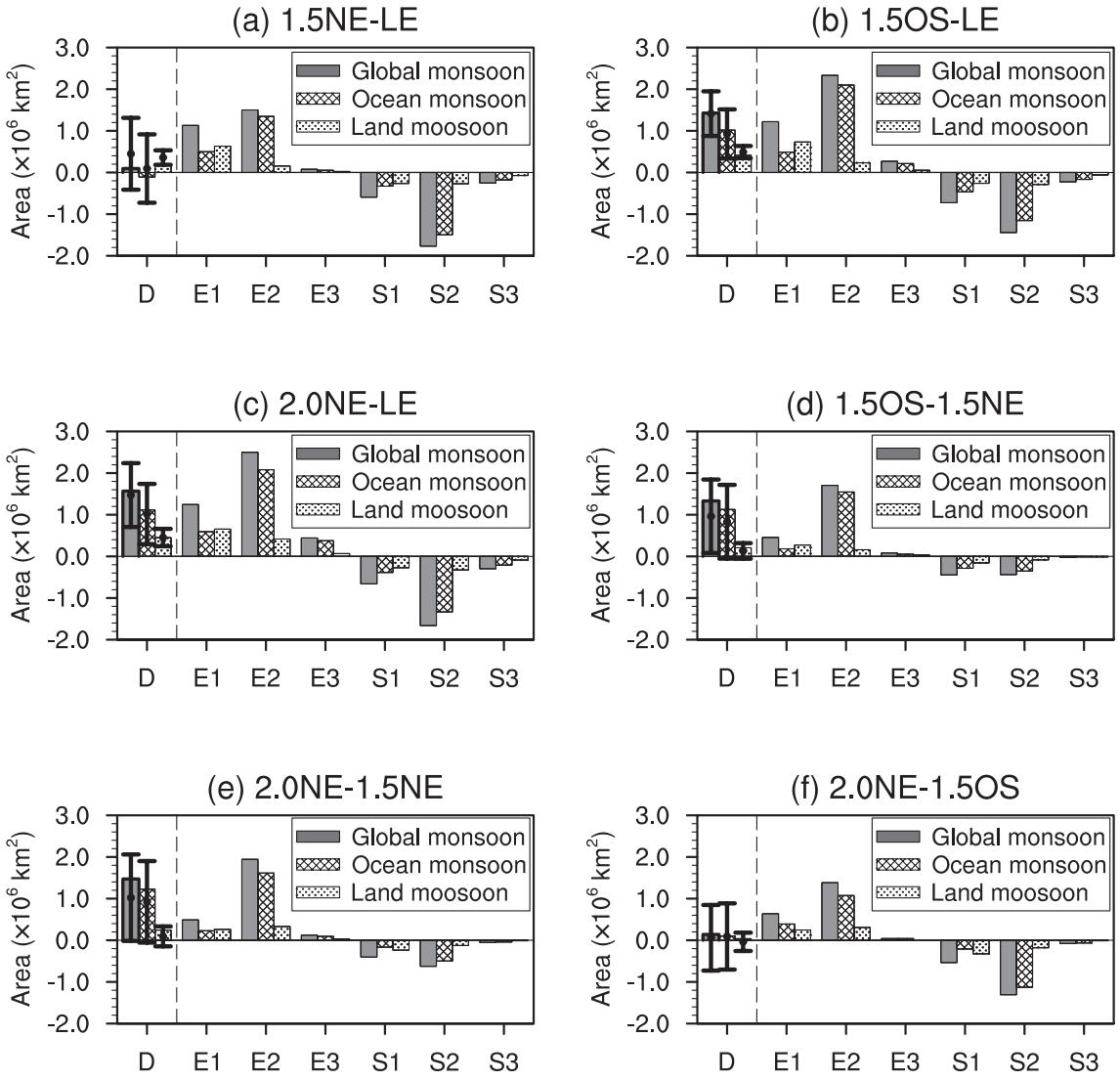

Fig. 2. GMA differences (units: 10^6 km^2) (a) between 1.5NE and LE, (b) between 1.5OS and LE, (c) between 2.0NE and LE, (d) between 1.5OS and 1.5NE, (e) between 2.0NE and 1.5NE, and (f) between 2.0NE and 1.5OS. The GMAs are based on the EM precipitation of each experiment. On the *x*-axis, D represents the corresponding GMA differences, E1 (S1) represents the GMA expansion (shrinkage) due to monsoon precipitation only, E2 (S2) represents the GMA expansion (shrinkage) due to the ratio of monsoon precipitation to annual precipitation only, and E3 (S3) represents the GMA expansion (shrinkage) due to both monsoon precipitation and the ratio. The results displayed in bars are computed by using "method 1". The gray, mesh and dotted bars respectively denote the results of the global, ocean and land monsoon. The solid dots and error bars are the corresponding GMA differences computed by using "method 2" and their 95% confidence intervals.

without exceeding them, the 0.5°C difference leads to a significance change in GMA (Fig. 2e).

To investigate the causes of the GMA change, we compare the GMAs of the scenarios. Consider the GMA change in 1.5NE relative to LE, for instance. First, we determine the area inside the GMA of 1.5NE but outside of the GMA of LE, named the "expansion area". Then, we classify the "expansion area" into three categories. (1) E1: This area expands due to GMR only. More precisely, in this area in the LE experiment, the percentage of monsoon precipitation is no less than 55% and the monsoon precipitation annual range is less than 2 mm d^{-1}; under the 1.5NE scenario, the percentage is still no less than 55% and the annual range increases to no less than 2 mm d^{-1}. (2) E2: The area expands due to GM percentage only. In the LE experiment, the monsoon precipitation annual range in E2 is no less than 2 mm d^{-1} and the percentage of monsoon precipitation is less than 55%; under the 1.5NE scenario, the annual range is still no less than 2 mm d^{-1}, and the percentage increases to no less than 55%. (3) E3: The area expands due to both GMR and the GM percentage. In the LE experiment, the monsoon precipitation annual range in E3 is less than 2 mm d^{-1} and the percentage of monsoon precipitation is less than 55%; under the 1.5NE scenario, the annual range increases to no less than 2 mm d^{-1}

and the percentage increases to no less than 55%. Similarly, we define the GMA shrinking area and classify the area into three categories named S1, S2 and S3. The changes in the specified areas are displayed as bars in Fig. 2. In all comparisons, the areas that occur due to GM percentage change are the greatest (see terms E2 and S2 in Fig. 2). The net changes due to GM percentage are approximately equal to the total GMA change. The contribution of monsoon precipitation annual range is second, and the contribution due to both GMR and the GM percentage is quite low.

Under a scenario of global warming, climate change is not spatially homogeneous. For example, due to the discrepant properties of Earth's surface (the low heat content of land and oceanic evaporation), surface temperature change in reponse to global warming is not uniform (Sutton et al., 2007). Global warming alters ocean dynamics, which may exert influence on atmospheric circulation and precipitation (Xie et al., 2010). In addition, heat storage by land is relatively low. In this light, during global warming, discrepancies may exist in the responses of the ocean and land monsoons.

For ocean monsoons, relative to present climate, scenarios 1.5OS and 2.0NE display significant areal changes, whereas scenario 1.5NE shows no significant change (Figs. 2a–c). It is qualitatively the same as the responses of the GMA. Among the three "future" scenarios, the monsoon areas display no significant changes (Figs. 2d–f). The above changes in the ocean monsoon area are mainly led by monsoon percentage change (see terms E2 and S2 in Fig. 2). More precisely, expansion or shrinkage of the oceanic monsoon areas are mainly controlled by monsoon percentage change, which causes more or less area to meet the criteria of monsoon.

For land monsoons, the features show some discrepancies. Relative to present climate, the monsoon areas in all the three "future" scenarios display significant changes, but the changes are less than those associated with ocean monsoons (Figs. 2a–c). This indicates that the land monsoon areas among the ensembles in each experiment vary little and that the ocean monsoon areas among the ensembles of each experiment display greater variances. Among the three "future" scenarios, the discrepancies are insignificant (Figs. 2d–f). For the land monsoon area change, the change in monsoon precipitation and monsoon precipitation percentage both affect the area, with the first factor slightly greater than the latter.

By comparing the land and ocean monsoons, it is found that the area change in ocean monsoons mainly accounts for the GMA change. For example, compare 2.0NE with LE. The area change in ocean monsoons contributes to 71% of the GMA change. That is, the expansion or shrinkage of the GMA mainly occurs over oceans.

Therefore, relative to the present day, the GMA change displays little change in the 1.5NE scenario and significant increases in the 1.5OS and 2.0NE scenarios. There is a significant increase in 2.0NE relative to 1.5NE. The above increases are mainly led by the GM percentage change. Furthermore, the GM percentage changes over ocean monsoon domains mainly account for the above GMA changes.

4.2. *GMP*

Using a method similar to "method 2" in section 4.1, we obtain the GMP and its confidence intervals. The results are shown in Fig. 3a. In 1.5NE, 1.5OS and 2.0NE, all GMP values significantly increase relative to the present day. The increases in GMP in the three scenarios are 0.18 mm d^{-1}, 0.19 mm d^{-1} and 0.24 mm d^{-1}, respectively, or relative increases of 2.9%, 3.1% and 3.9%. Little change is observed between 1.5NE and 1.5OS, indicating that different trajectories reaching the goal of a 1.5°C GMT increase in 2100 make no difference in terms of GMP. Relative to the 1.5°C temperature goal, the GMP under the 2.0°C temperature goal increases significantly (approximately 0.06 mm d^{-1}).

The scales of the patterns of GMP change generally meet the scales of the GMP. The patterns of GMP change in the

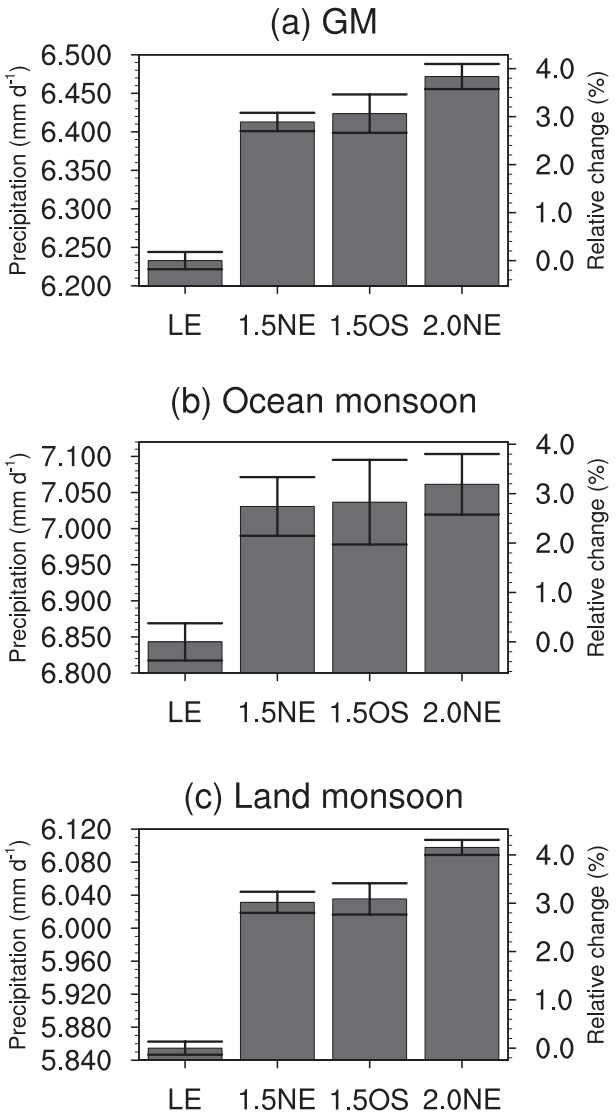

Fig. 3. The (a) GMP, (b) ocean monsoon precipitation and (c) land monsoon precipitation (units: mm d^{-1}) of the scenarios. Bars indicate the EMs and error bars display the 95% confidence intervals. The area averages of monsoon precipitation over the GMAs are first calculated in each ensemble, and then the confidence intervals are obtained in each experiment.

three "future" scenarios relative to the present day are similar (Fig. 4). It is interesting that the enhanced precipitation over the Asian monsoon domain is more prominent than that over other monsoon areas.

As GMAs change in the future, do such changes affect the GMP? To study the influences, we first compute the EM of the precipitation for each experiment; then, we obtain the GMP in each experiment, and the difference between the future and the present day is called "precipitation with GMA change". Then, we compute the average of the monsoon precipitation change over the areas that belong to the GMAs in both future and present-day climate. We call these results "precipitation without GMA change". Finally, the effect of GMA change on GMP is obtained by comparing the precipitation "with" and "without" GMA change. The GMA effect on GMP change is the strongest in 1.5OS compared to LE. The GMA change contributes to 0.02 mm d^{-1}, which is approximately 10% of the precipitation change and is 0.3% of the GMP in present-day climate. The effects of GMA change on GMP are negligible. The change in ocean monsoon area accounts for approximately one-third of ocean monsoon precipitation; the effect on the change in land monsoon area is negligible (figures not shown). This is consistent with the fact that the area change in ocean monsoons is greater than that of land monsoons.

To understand the dynamic structure of the GMP change, a diagnostic analysis of the moisture budget is performed. Following Chou et al. (2009), the precipitation in anomaly form is

$$P' = -\langle \bar{\omega}\partial_p q' \rangle - \langle \omega' \partial_p \bar{q} \rangle - \langle \overline{\boldsymbol{V}} \cdot \nabla q' \rangle - \langle \boldsymbol{V}' \cdot \nabla \bar{q} \rangle + E', \quad (2)$$

where the overbars and primes denote reference states and changes relative to reference states, respectively; P, ω, q, $\boldsymbol{V}$ and E respectively represent the precipitation, pressure velocity, specific humidity, horizontal wind vector and evaporation; and $\langle\ \rangle$ denotes a mass integration from the surface to 100 hPa.

As the GMA changes affect GMP very little, we analyze the moisture budget over the GMA belonging to both the two comparable experiments. For example, if we diagnose the moisture budget equation of the 1.5NE scenario relative to LE, we focus on the shared GMA in 1.5NE and LE. Here, the analysis is based on "method 1", and the results are displayed in Fig. 5. In all of the comparisons, the qualitative conclusion is the same: the GMP change is mainly affected by the change in the vertical gradient of specific humidity and the change

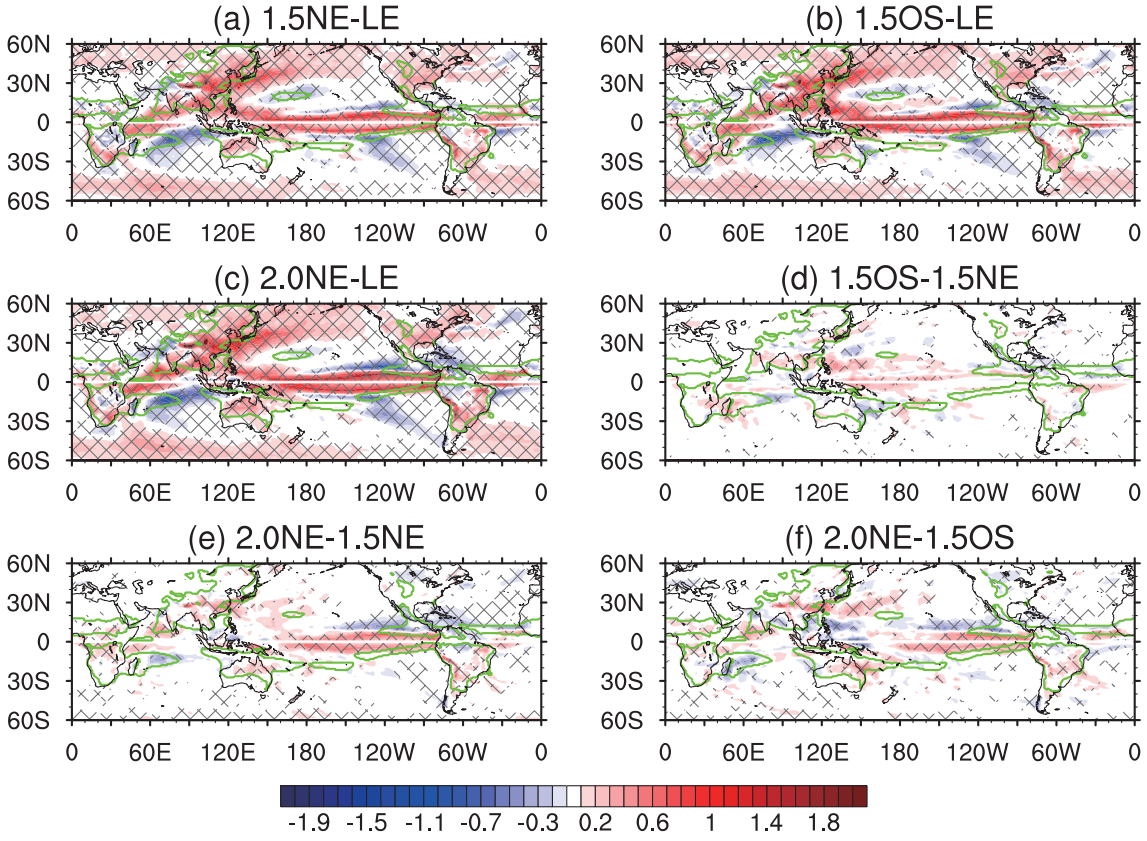

Fig. 4. The differences (units: mm d^{-1}) in GMP between (a) 1.5NE and LE, (b) 1.5OS and LE, (c) 2.0NE and LE, (d) 1.5OS and 1.5NE, (e) 2.0NE and 1.5NE, and (f) 2.0NE and 1.5OS. The green contours are the outlines of the GMAs. In (a–c), the GMAs are the results of the LE EM; in (d, e), the GMAs are the results of the 1.5NE EM; in (f), the GMA is the result of the 1.5OS EM. The GMP is the local summer mean result, where local summer is May to September in the Northern Hemisphere and November to March in the Southern Hemisphere. Lattices indicate that the confidence level of the results reaches 90%.

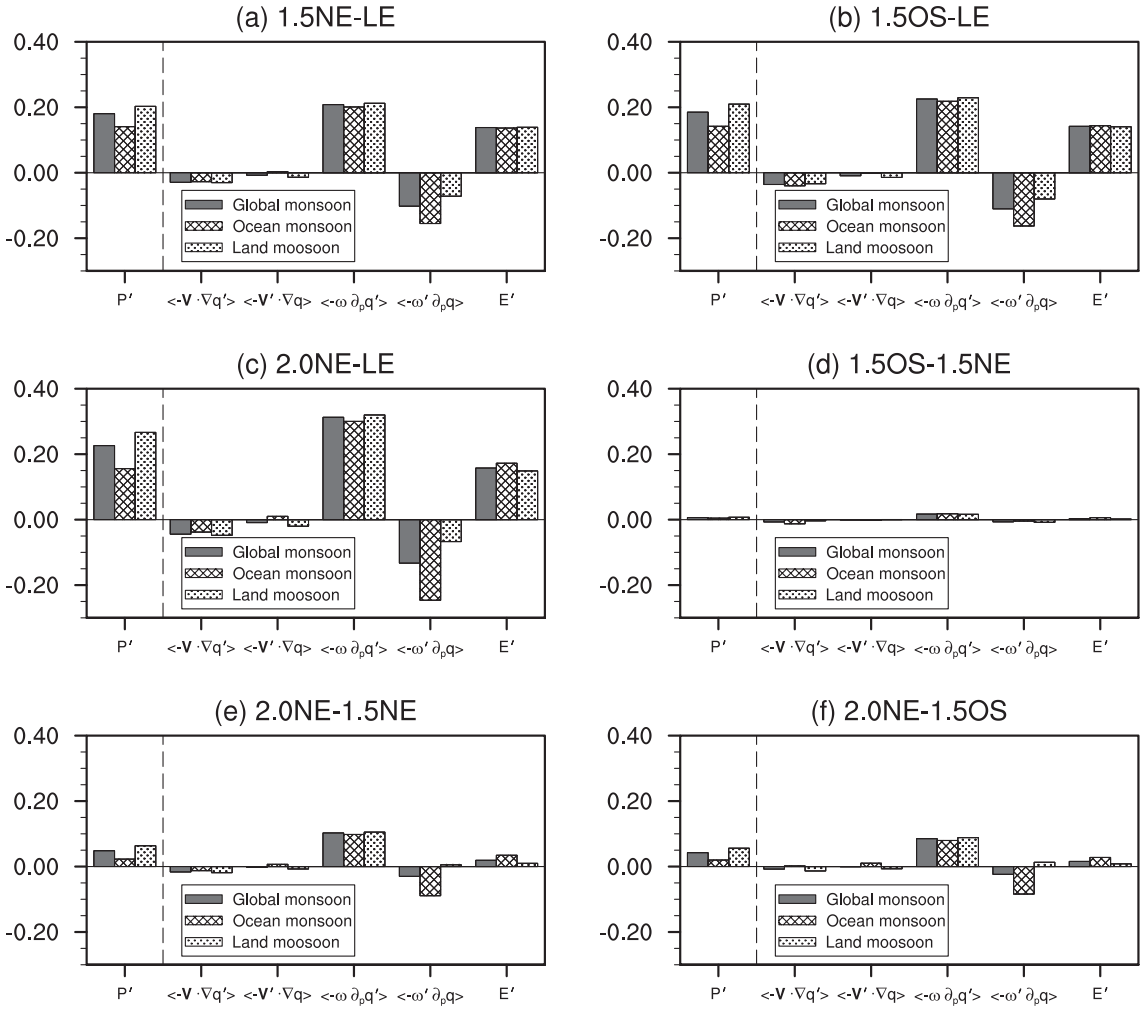

Fig. 5. Area-averaged terms of the moisture budget equation associated with GMP in (a) 1.5NE relative to LE, (b) 1.5OS relative to LE, (c) 2.0NE relative to LE, (d) 1.5OS relative to 1.5NE, (e) 2.0NE relative to 1.5NE, and (f) 2.0NE relative to 1.5OS. The terms are displayed on the x-axis. The units are mm d^{-1}. The associated GMAs and the variables are calculated using "method 1". The gray, mesh and dotted bars respectively denote the results of global, ocean and land monsoon.

in evaporation. The change in the vertical gradient of specific humidity is mainly due to the enhancement of specific humidity led by surface warming. For evaporation change, the lack of surface specific humidity in the output makes the evaluation of reasons for evaporation change difficult. Inferred from the results in Hsu et al. (2013), the evaporation change over the GMA may be mainly caused by the change in the humidity difference between the surface and air. The change in the vertical velocity makes an opposite-sign contribution. Over the GM domains, the vertical motion is dominated by ascendance. Under a warming scenario, the atmospheric circulation tends to slow (Held and Soden, 2006), which means that the ascending motion over the GM domains weakens. It partly cancels out the increase in precipitation. At the same time, horizontal moisture advection contributes little to the GMP change. Our GMP responses share the same mechanism as those under global warming revealed by Kitoh et al. (2013), Hsu et al. (2013), Endo and Kitoh (2014), and Endo et al. (2018).

Over the Asian monsoon area, our results are similar to those in Lee et al. (2018). They examined the Asian monsoon response between 1.5°C and 2°C target experiments using five atmospheric global climate models forced by designated sea surface temperature, sea ice, aerosols and GHGs. It implies that the air–sea interaction may contribute quite little to the monsoon rainfall increases.

Relative to present-day climate, the behaviors of ocean monsoon precipitation changes are similar to those of GMP change. The three "future" scenarios all display significant increases (significance level exceeding 99%) in ocean monsoon precipitation (Fig. 3b). The increases in the three "future" scenarios are similar and have insignificant differences. A moisture budget diagnosis is performed on ocean and land monsoons. The results are similar to those for the GMP change. The change in ocean monsoon precipitation is mainly controlled by the enhancement of humidity and evaporation under a warming climate (Fig. 5). Changes in ascending motion have opposite-sign contributions.

The behaviors of land monsoon changes in the future relative to present-day climate are similar to those of ocean monsoons (Fig. 3c). However, the change in land monsoon precipitation in 2.0NE is significantly different than that in 1.5NE and 1.5OS. Similar to ocean monsoon precipitation, land monsoon precipitation change is mainly controlled by the enhancement of humidity and evaporation, which is induced by global warming; the vertical motion change partly offsets the increase in precipitation (Fig. 5). Compared to the magnitudes of ocean monsoon precipitation changes, the land monsoon differs in the following ways: (1) the land-averaged increases in monsoon precipitation are greater than ocean-averaged increases; (2) regardless of the sign, the contribution of vertical motion change on land monsoon precipitation change is less than that on ocean monsoon precipitation change. It is easy to understand that, over land monsoon areas, the greater increase in mean precipitation is mainly due to less of a weakening in the ascending motion.

Figure 6 displays the differences of ω at 500 hPa between the given two experiments. In the three "future" scenarios, all monsoon areas display a dominant descending response, except the Asian monsoon area (Figs. 6a–c). From the southeastern Tibetan Plateau to South China, enhanced ascending motion is observed. This makes the increase in local monsoon precipitation stronger than in other monsoon areas. The enhanced ascending motion may be the consequence of enhanced moisture convergence caused by the strengthening of the North Pacific anticyclonic circulation under a warming climate (Seo and Ok, 2013; Wang et al., 2013). No large-scale enhancement of ascending motion is observed over ocean monsoon areas. Thus, this large-scale ascending motion enhancement results in the land–ocean difference in the increase in monsoon precipitation.

Therefore, relative to present-day climate, the GM, ocean and land monsoon precipitation significantly increase under the two 1.5°C scenarios and an additional significant increase is found in the results of the GMP and land monsoon precipitation under the 2.0NE scenario. The monsoon area changes affect the increase in GMP and land monsoon precipitation very little. The increases in GM, ocean and land monsoon precipitation are mainly due to the enhancement of humidity and evaporation, whereas weakened ascending motion partly cancels out the increase in the monsoon precipitation. However, the overall ascending motion weakens less in land monsoon areas than than in ocean monsoon areas, leading the overall incease in land monsoon precipitation to be greater than that in ocean monsoon precipitation.

4.3. *Monsoon rainfall percentage*

Similar to the calculation of GMP differences, we compute the differences in GM percentage. The corresponding results are displayed in Fig. 7. The GM percentage differences are no greater than 0.32%, which is low relative to the averaged GM percentage (71.4%) in a present-day climate.

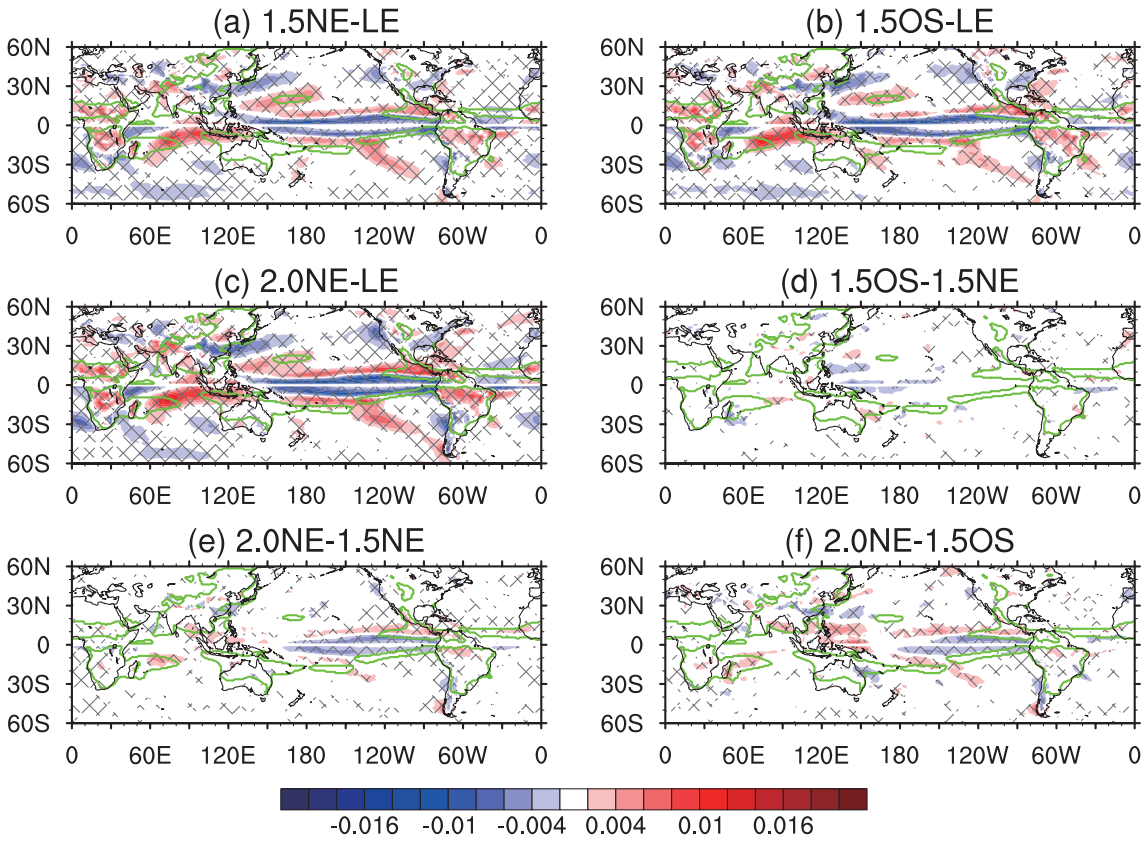

Fig. 6. As in Fig. 4. but for the differences of ω at 500 hPa. Units: Pa s^{-1}.

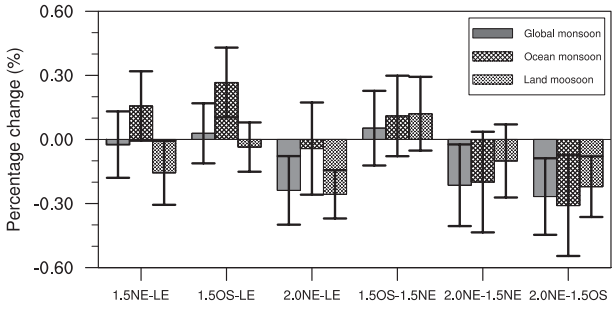

Fig. 7. Differences of GM (gray bars), ocean monsoon (mesh bars) and land monsoon (dotted bars) percentage (units: %) between the given two scenarios. On the *x*-axis, for example, 1.5NE-LE means the corresponding percentage in the 1.5NE scenario minus that in the LE experiment. The calculation is based on "method 2". The error bars displays the 95% confidence intervals.

This means that the ratios of the monsoon precipitation (also the local summer precipitation) to annual precipitation barely change in the "future".

On a regional scale, the scale of GM percentage change is approximately 1%. Consider the difference between 2.0NE and 1.5NE, for example. The percentage difference varies from −10.7% to 9.1% (figures not shown). The negligible changes in GM percentage in future scenarios implies that no consistent percentage change over the GMA occurs.

In addition, it can be implied from the negligible changes in GM percentage that the increase in the area-average local winter precipitation over the GMA is the same percentage as local summer precipitation (monsoon precipitation). For the global average, since the local winter precipitation is less than local summer precipitation, an increase in both of the same percentage leads to an increase in the GMR.

Similar results are found for ocean and land monsoons. For both types of monsoon, the monsoon precipitation percentage barely changes in all scenarios (Fig. 7). It can be inferred that, for both land and ocean monsoons, local winter precipitation and monsoon annual range both increase.

4.4. *Monsoon onset and withdrawal*

Similar to the work of Lee and Wang (2014), the onset month of the summer monsoon is defined as the first month of local summer, which is May in the Northern Hemisphere and November in the Southern Hemisphere. The withdrawal month is defined as the last month of local summer, which is September in the Northern Hemisphere and March in the Southern Hemisphere. The global mean precipitation change over the GMA during the onset and withdrawal months is tightly associated with the onset and withdrawal of the GM, respectively. For example, if the precipitation increases in both the onset and withdrawal months, it indicates an earlier onset and postponed withdrawal.

Under the scenarios proposed in the Paris Agreement, the GM onset remains generally unchanged. In both the 1.5NE and 1.5OS scenarios, the precipitation in the monsoon onset month increases insignificantly (Fig. 8). In the 2.0NE scenario, the precipitation change in the monsoon onset month is significant, with an increase of 0.05 mm d^{-1}, which is quite low relative to the corresponding GMP change. The GMA change largely affects the monsoon precipitaiton in the onset month. If the rainfall changes over the shared area of the GMAs in the 2.0NE and LE experiments are compared, the increase is 0.02 mm d^{-1}. The small increase in rainfall over the shared area of the GMAs is mainly caused by the offset of three terms: $-\langle\bar{\omega}\partial_p q'\rangle$, $-\langle\omega'\partial_p\bar{q}\rangle$ and E' (figures not shown).

The postponed GM withdrawal will occur under the scenarios proposed in the Paris Agreement. Figure 8a displays the precipitation differences in the monsoon withdrawal month between the two experiments. Relative to LE, all future scenarios display a significant precipitation increase

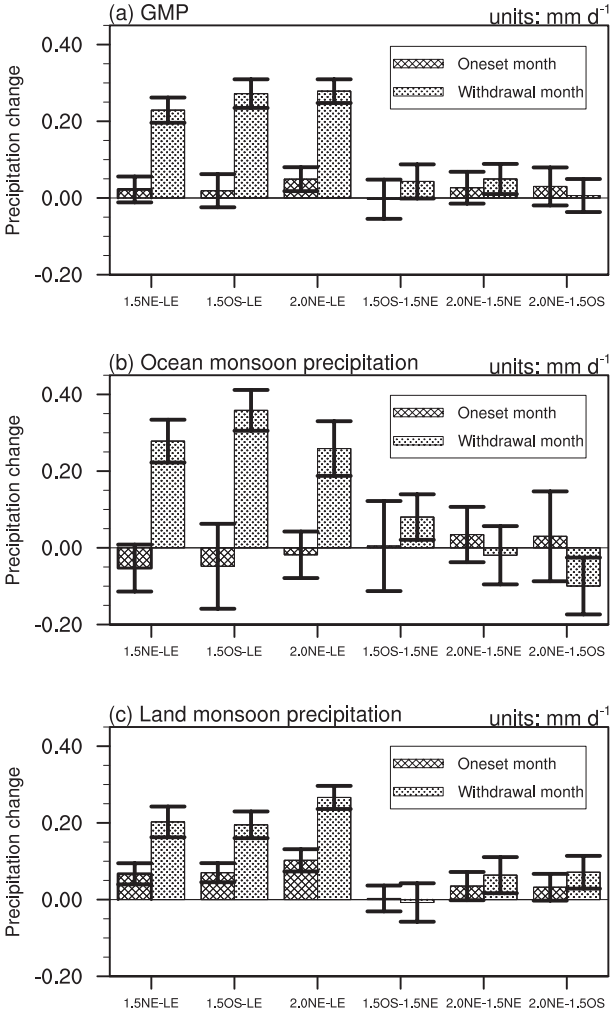

Fig. 8. Area-averaged precipitation change in monsoon onset (mesh bars) and withdrawal (dotted bars) months over the GMAs. Units: mm d^{-1}. Panels (a–c) are the results of the GM, ocean monsoon and land monsoon, respectively. On the *x*-axis, for example, 1.5NE-LE means GMP in the 1.5NE scenario minus GMP in the LE experiments. The error bars are the 95% confidence intervals of the corresponding differences. The calculation is based on "method 2".

(exceeding the 99% significance level) in the monsoon withdrawal month. The increase is close to the magnitude of GMP change. This means that the monsoon withdrawal will be delayed. For precipitation change in the monsoon withdrawal month, the GMA change contributes little (figures not shown). Similar to the method presented in section 4.2, the moisture budget is determined, and the results are displayed in Fig. 9. The results reflect that the precipitation increase is also mainly affected by the enhancement of humidity and evaporation and that the global warming–induced weakening in ascending motion makes an opposite-sign contribution.

Additionally, a weak postponement of monsoon withdrawal may occur under the 2.0NE scenario compared to the 1.5NE scenario. The precipitation difference in the monsoon withdrawal month is 0.05 mm d^{-1}, reaching the 95% significance level (Fig. 8a). The GMA change affects the precipitation difference very little (figures not shown). The moisture budget analysis indicates that the precipitation difference is mainly affected by an enhancement of humidity and that the weakening ascending motion also provides an opposite-sign contribution (Fig. 9e).

The onset of both land and ocean monsoons is unlikely to advance. In the monsoon onset month, the change in precipitation is quite small (Figs. 8b and c). The maximum precipitation change is the land monsoon change in 2.0NE compared to LE at approximately 0.1 mm d^{-1}. It is less than half of the corresponding change during the withdrawal month.

Relative to present-day climate, in monsoon withdrawal months, the three "future" scenarios all display significant increases (significance level exceeding 99%) for both ocean and land monsoon (Figs. 8b and c). The increases in magnitude are not consistent between land and ocean monsoons. In 1.5NE and 1.5OS relative to LE, the averaged increase in ocean precipitation is geater than that of land precipitation over the GMAs in monsoon withdrawal months; the results are the reverse in 2.0NE relative to LE. Among the three "future" scenarios, the discrepancies are quite small. The results of the moisture budget analysis are similar to those of the GMP results in withdrawal months. The enhancements of humidity and evaporation contribute to the increases in precipitation in withdrawal months, whereas the weakening of vertical motion over the monsoon areas partly cancels out the increases in precipitation (Figs. 9a–c).

Over land monsoon areas, two competing mechanisms affect the precipitation responses to global warming (Seth et al., 2013). One is the local mechanism; that is, the surface

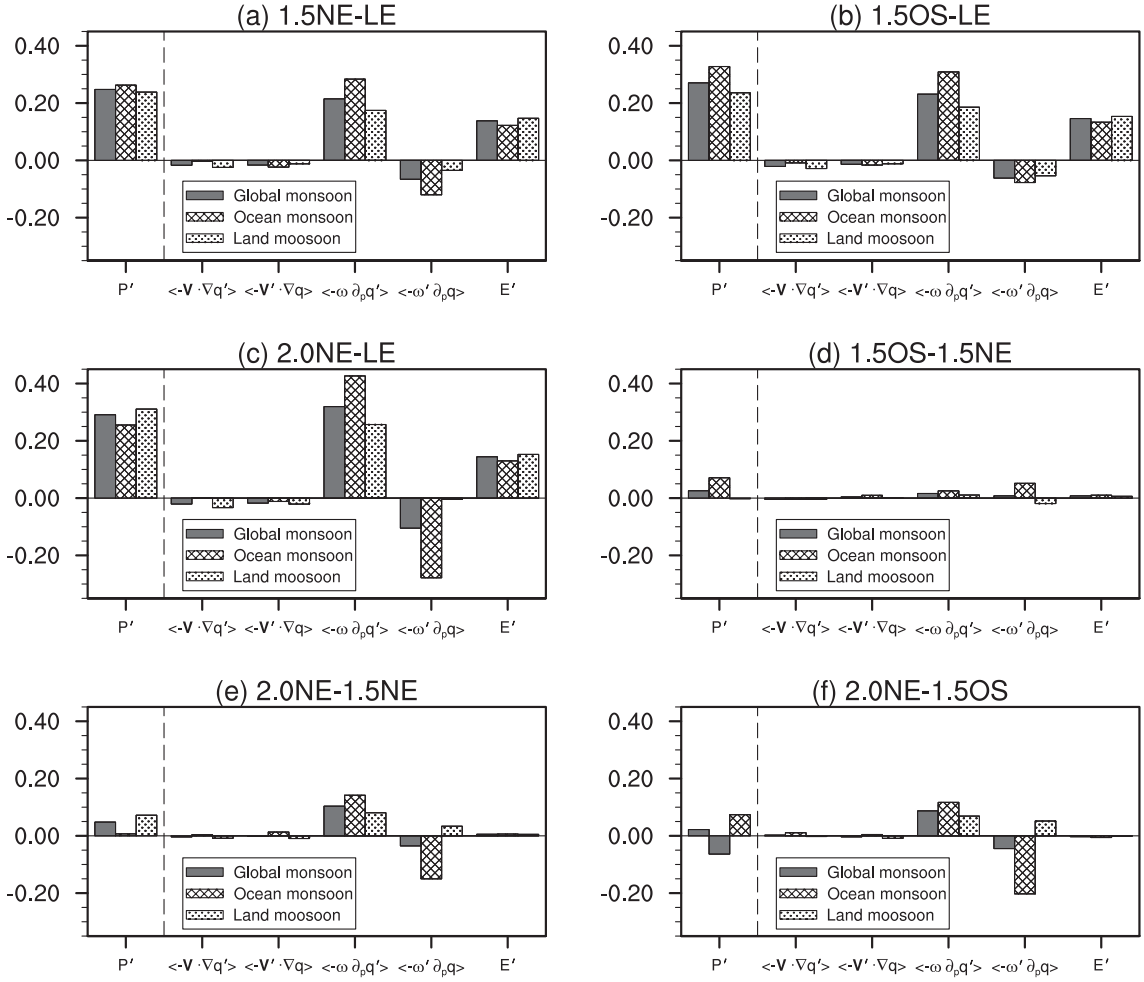

Fig. 9. As in Fig. 5. but for the moisture analysis in monsoon withdrawal months.

warming over land leads to more moisture near the surface, increases low-level moist static energy and dereases the stability. The other is the remote mechanism; that is, in the tropics, the ocean warming may lead to a warmed troposphere over land and increases the stability over land. During the monsoon onset months, the two mechanisms compete, leading to the small change in land monsoon precipitation; during the monsoon withdrawal months, the local mechanism dominates, leading to the larger increases in land monsoon precipitation.

Therefore, the length of the GM, ocean monsoon and land monsoon in each year is possibly prolonged due to their postponed withdrawal.

5. Summary and discussion

Based on CESM1(CAM5) experiments and GPCP and CMAP data, using spatial correlation and reproducibility evaluation, the GM features in CESM1(CAM5) are evaluated. The features include the patterns of monsoon precipitation and monsoon domains, as well as the magnitudes of GMP, GMA, GM percentage and GMR. Based on the evaluation, it is viable to use CESM1(CAM5) to discuss all the above features except GMR.

GMA changes insignificantly in the 1.5NE scenario, and shows a significant increase in the 1.5OS and 2.0NE scenarios. Also, there is a significant increase in 2.0NE relative to 1.5NE. The GM percentage change mainly leads to the above GMA increases. The GMA changes in future scenarios are mainly controlled by changes in the ocean monsoon domain, which also results from the GM percentage change. The effect of a change in land monsoon area is weaker, and the change in area of land monsoons is controlled by changes in both monsoon precipitation and monsoon precipitation percentage, with the first factor generally greater than the latter.

GMP significantly increases under the two 1.5°C scenarios (1.5NE and 1.5OS) relative to present-day climate, and a significant additional increase is found under the 2.0NE scenario. The GMA changes affect GMP increases very little. The GMP increases are mainly due to the enhancement of humidity and evaporation, whereas weakened ascending motion partly cancels out the increase in GMP. For ocean monsoons, the area change accounts for approximately one-third of ocean monsoon precipitation; for land monsoons, the effects of area change are negligible. For both ocean and land monsoons, the results of the moisture budget analysis are qualitatively the same as those for GMP. Additional findings include: (1) the land-averaged increases in monsoon precipitation are greater than the ocean-averaged increase; and (2) the magnitude of the effect of vertical motion change on land monsoon precipitation change is less than that of the ocean monsoon precipitation change. Large-scale ascending motion enhancement is observed over the southeastern Tibetan Plateau to South China, leading to generally less of a weakening of mean ascending motion over land than over oceans. Consequently, the increase in land monsoon precipitation is greater than ocean monsoon precipitation.

In the future climates, the GM percentage changes little, from which we can infer that local winter precipitation and the annual range of monsoon precipitation may increase. Without exception, the land and ocean monsoons display the same results.

In the future scenarios, precipitation does not significantly change in the monsoon onset month, but significantly increases in the monsoon withdrawal month. The increases in the monsoon withdrawal month are mainly controlled by the enhancement of humidity and evaporation. Inferred from the precipitation results, the GM length in each year may be significantly prolonged. The land and ocean monsoons also display the same results.

Since the western North Pacific monsoon region is not reasonably simulated, we also used the GMA and observational results to investigate the GM changes. We repeated our investigation of the monsoon features over the GMA in both the GPCP and CMAP data. The conclusions were the same as those listed above (figures not shown).

The results here are gained based on ensembles of a single model output, in which the influence of the model's systematic bias may be larger than that of the multi-model approach. If more coupled global climate models conduct the 1.5NE, 1.5OS and 2.0NE experiments, multi-model ensembles of the models' outputs should yield results that are more trustworthy.

Acknowledgements. The authors wish to thank the two anonymous reviewers for their insightful comments, which led to a significant improvement in the manuscript. The study was supported by the National Natural Sciences Foundation of China (Grant Nos. 41530425 and 41425019).

REFERENCES

Adler, R. F., Coauthors, 2003: The version-2 global precipitation climatology project (GPCP) monthly precipitation analysis (1979–present). *Journal of Hydrometeorology,* **4**, 1147–1167, https://doi.org/10.1175/1525-7541(2003)004<1147:TVGPCP>2.0.CO;2.

Chadwick, R., P. L. Wu, P. Good, and T. Andrews, 2013: Asymmetries in tropical rainfall and circulation patterns in idealised CO_2 removal experiments. *Climate Dyn.*, **40**, 295–316, https://doi.org/10.1007/s00382-012-1287-2.

Chou, C., J. D. Neelin, C. A. Chen, and J. Y. Tu, 2009: Evaluating the "rich-get-richer" mechanism in tropical precipitation change under global warming. *J. Climate*, **22**, 1982–2005, https://doi.org/10.1175/2008JCLI2471.1.

Endo, H., and A. Kitoh, 2014: Thermodynamic and dynamic effects on regional monsoon rainfall changes in a warmer climate. *Geophys. Res. Lett.*, **41**, 1704–1711, https://doi.org/10.1002/2013GL059158.

Endo, H., A. Kitoh, and H. Ueda, 2018: A unique feature of the Asian summer monsoon response to global warming: The role of different land-sea thermal contrast change between the lower and upper troposphere. *Sola*, **14**, 57–63, https://doi.org/10.2151/sola.2018-010.

Good, P., B. B. B. Booth, R. Chadwick, E. Hawkins, A. Jonko, and J. A. Lowe, 2016: Large differences in regional precipitation change between a first and second 2 K of global warming. *Nature Communications*, **7**, 13667, https://doi.org/10.1038/ncomms13667.

Held, I. M., and B. J. Soden, 2006: Robust responses of the hydrological cycle to global warming. *J. Climate*, **19**, 5686–5699, https://doi.org/10.1175/JCLI3990.1.

Held, I. M., M. Winton, K. Takahashi, T. Delworth, F. R. Zeng, and G. K. Vallis, 2010: Probing the fast and slow components of global warming by returning abruptly to preindustrial forcing. *J. Climate*, **23**, 2418–2427, https://doi.org/10.1175/2009JCLI3466.1.

Hirota, N., Y. N. Takayabu, M. Watanabe, and M. Kimoto, 2011: Precipitation reproducibility over tropical oceans and its relationship to the double ITCZ problem in CMIP3 and MIROC5 climate models. *J. Climate*, **24**, 4859–4873, https://doi.org/10.1175/2011JCLI4156.1.

Hsu, P. C., T. Li, and B. Wang, 2011: Trends in global monsoon area and precipitation over the past 30 years. *Geophys. Res. Lett.*, **38**, L08701, https://doi.org/10.1029/2011GL046893.

Hsu, P. C., T. Li, H. Murakami, and A. Kitoh, 2013: Future change of the global monsoon revealed from 19 CMIP5 models. *J. Geophys. Res.*, **118**, 1247–1260, https://doi.org/10.1002/jgrd.50145.

Kay, J. E., Coauthors, 2015: The Community Earth System Model (CESM) large ensemble project: A community resource for studying climate change in the presence of internal climate variability. *Bull. Amer. Meteor. Soc.*, **96**, 1333–1349, https://doi.org/10.1175/BAMS-D-13-00255.1.

Kitoh, A., H. Endo, K. K. Kumar, I. F. A. Cavalcanti, P. Goswami, and T. J. Zhou, 2013: Monsoons in a changing world: A regional perspective in a global context. *J. Geophys. Res.*, **118**, 3053–3065, https://doi.org/10.1002/jgrd.50258.

Lee, D., S.-K. Min, E. Fischer, H. Shiogama, I. Bethke, L. Lierhammer, and J. F. Scinocca, 2018: Impacts of half a degree additional warming on the Asian summer monsoon rainfall characteristics. *Environmental Research Letters*, **13**, 044033, https://doi.org/10.1088/1748-9326/aab55d.

Lee, J. Y., and B. Wang, 2014: Future change of global monsoon in the CMIP5. *Climate Dyn.*, **42**, 101–119, https://doi.org/10.1007/s00382-012-1564-0.

Long, S. M., S. P. Xie, X. T. Zheng, and Q. Y. Liu, 2014: Fast and slow responses to global warming: Sea surface temperature and precipitation patterns. *J. Climate*, **27**, 285–299, https://doi.org/10.1175/JCLI-D-13-00297.1.

Sanderson, B. M., B. C. O'Neill, and C. Tebaldi, 2016: What would it take to achieve the Paris temperature targets? *Geophys. Res. Lett.*, **43**, 7133–7142, https://doi.org/10.1002/2016GL069563.

Sanderson, B. M., Coauthors, 2017: Community climate simulations to assess avoided impacts in 1.5°C and 2°C futures. *Earth System Dynamics*, **8**, 827–847, https://doi.org/10.5194/esd-8-827-2017.

Seo, K. H., and J. Ok, 2013: Assessing future changes in the East Asian summer monsoon using CMIP3 Models: Results from the best model ensemble. *J. Climate*, **26**, 1807–1817, https://doi.org/10.1175/JCLI-D-12-00109.1.

Seth, A., S. A. Rauscher, M. Biasutti, A. Giannini, S. J. Camargo, and M. Rojas, 2013: CMIP5 projected changes in the annual cycle of precipitation in monsoon regions. *J. Climate*, **26**, 7328–7351, https://doi.org/10.1175/JCLI-D-12-00726.1.

Sutton, R. T., B. W. Dong, and J. M. Gregory, 2007: Land/sea warming ratio in response to climate change: IPCC AR4 model results and comparison with observations. *Geophys. Res. Lett.*, **34**, L02701, https://doi.org/10.1029/2006GL028164.

Taylor, K. E., 2001: Summarizing multiple aspects of model performance in a single diagram. *J. Geophys. Res.*, **106**, 7183–7192, https://doi.org/10.1029/2000JD900719.

UNFCCC, 2015: *Adoption of the Paris Agreement*. UNFCCC.

Wang, B., and Q. H. Ding, 2008: Global monsoon: Dominant mode of annual variation in the tropics. *Dyn. Atmos. Oceans*, **44**, 165–183, https://doi.org/10.1016/j.dynatmoce.2007.05.002.

Wang, B., S. Y. Yim, J. Y. Lee, J. Liu, and K. J. Ha, 2013: Future change of Asian-Australian monsoon under RCP 4.5 anthropogenic warming scenario. *Climate Dyn.*, **42**, 83–100, https://doi.org/10.1007/s00382-013-1769-x.

Wang, G. J., W. J. Cai, B. L. Gan, L. X. Wu, A. Santoso, X. P. Lin, Z. H. Chen, and M. J. McPhaden, 2017: Continued increase of extreme El Niño frequency long after 1.5°C warming stabilization. *Nat. Clim. Change*, **7**, 568–572, https://doi.org/10.1038/nclimate3351.

Xie, P. P., and P. A. Arkin, 1997: Global precipitation: a 17-year monthly analysis based on gauge observations, satellite estimates, and numerical model outputs. *Bull. Amer. Meteor. Soc.*, **78**, 2539–2558, https://doi.org/10.1175/1520-0477(1997)078<2539:GPAYMA>2.0.CO;2.

Xie, S. P., C. Deser, G. A. Vecchi, J. Ma, H. Y. Teng, and A. T. Wittenberg, 2010: Global warming pattern formation: Sea surface temperature and rainfall. *J. Climate*, **23**, 966–986, https://doi.org/10.1175/2009JCLI3329.1.